J. Appl. Comput. Mech., xx(x) (2026) 1-14
DOI: 10.22055/jacm.2025.48377.5191

ISSN: 2383-4536
jacm.scu.ac.ir

Shahid Chamran University of Ahvaz

Journal of Applied and Computational Mechanics

Research Paper

On the $\mathscr{L}_1$ Norm Minimization in Adaptive Control of Launch Vehicles

Naji Anees Muqdad Naji[1], Adrian-Mihail Stoica[2]

[1] Doctoral School of Aerospace Engineering, National University of Science and Technology Politehnica of Bucharest, Str. Gh. Polizu 1-7, Bucharest, Romania, Email: anees.naji@stud.aero.upb.ro

[2] Department of Aeronautical Systems Engineering and Aeronautical Management" Nicolae Tipei", National University of Science and Technology Politehnica of Bucharest, Str. Gh. Polizu 1-7, Bucharest, Romania, Email: adrian.stoica@upb.ro

Received April 19 2025; Revised December 27 2025; Accepted for publication December 29 2025.
Corresponding author: N.A.M. Naji (anees.naji@stud.aero.upb.ro)

Abstract. The present paper analyses an $\mathscr{L}_1$ adaptive control procedure for the control of launch vehicles. A crucial step in the $\mathscr{L}_1$ adaptive control design methodology is the minimization of the $\mathscr{L}_1$-norm of a specific system, which depends on the launcher model and a stable filter. The lower this norm is, the better it guarantees robustness properties with respect to modeling uncertainties and parameter variations of the launcher dynamics. The paper focuses on determining a numerically reliable methodology for minimizing this norm. It is proven that the parameters of the optimal $\mathscr{L}_1$ adaptive controller may be obtained by solving a specific system of matrix inequalities. The proposed procedure is illustrated and validated by a case study for the VEGA launch vehicle.

Keywords: $\mathscr{L}_1$ adaptive controller, Rigid and flexible models of the launch vehicle, Parametric modeling uncertainties, System of matrix inequalities.

1. Introduction

The control of the pitch and yaw motion of modern launch vehicles during their atmospheric flight is typically performed using a Thrust Vectoring Control (TVC) system. The nozzle deflection is determined by specific control laws, implemented in the onboard computer, based on measurements provided by the Inertial Navigation System (INS). These control laws must provide a wide variety of performance objectives, including vehicle stabilization, accurate tracking of the desired trajectory, attenuation of the atmospheric disturbances' effects, load and drift management, and robustness concerning modeling uncertainties and parameter variations. The design of launchers' automatic flight control systems is a challenging task due to the fast variation of the dynamics parameters during the ascent phase of flight. Moreover, stability performance severely degrades in the presence of inherent structural flexible effects. Due to the continuous diversification of space missions over the last decades, many design procedures for the design of launchers' control systems have been recently proposed and investigated. They include a wide variety of methods, starting with the classical Proportional-Integral-Derivative (PID) controller [1-4], continuing with modern optimal methods as LQG (Linear Quadratic Gaussian) control [5-7] and H_∞-norm minimization-based techniques [8-10] to mention just a few design methodologies used for the TVC system. A key problem in the implementation of these control systems is the change of their parameters as a function of the flight conditions. Usually, this problem is addressed using a "gain scheduling" approach in which the control laws' parameters are periodically adjusted based on navigation data. An alternative approach with an old history in aviation, but with fewer applications for launch vehicles, is to use adaptive control systems [11, 12] for launcher applications. Such control systems provide an "auto-tuning" of their parameters depending on the flight conditions. Although such solutions are suitable for many applications where flight conditions change, their use for launch vehicles was limited due to the rapid changes in dynamic parameters during atmospheric flight. A reliable solution to ensure fast adaptation while providing good robustness, stability, and performance in the presence of rapid changes of the launcher dynamics parameters is based on the so-called $\mathscr{L}_1$ adaptive control [13-15]. The main idea behind this approach is that by minimizing the $\mathscr{L}_1$-norm of a particular system, depending on the vehicle model and a stable filter, one may increase the stability radius of the resulting system in the presence of parametric modeling uncertainties.

The $\mathscr{L}_1$-norm minimization algorithm is integrated in this paper with a linear controller derived through control methods commonly used to accomplish the requirements for flight, resulting thus an overall nonlinear control system. Moreover, the previous applications of the $\mathscr{L}_1$ adaptive control include reduced order filters which parameters are determined by direct search methods.

The main contributions of the present paper include:

• Development of an adaptive augmented control algorithm based on the $\mathscr{L}_1$-norm minimization of the pitch/yaw motion of a launch vehicle.

Published online: January 01 2026

• An optimization procedure allowing the determination of the filter used in the $\mathscr{L}_1$-norm minimization methodology. This procedure aims to minimize the $\mathscr{L}_1$-norm for the case when such filters have an arbitrary prescribed order. It represents a generalization of the commonly used approaches in which the filter parameters are determined by direct search methods.

• Verification and validation of the feasibility of the adaptive control algorithm considering flexible modes effects, actuator dynamics, time delay, and atmospheric disturbances for the pitch/yaw dynamics of the European VEGA launcher.

The paper is organized as follows: the next section presents some preliminary definitions, results, and considerations regarding the $\mathscr{L}_1$-norm. In the third section, the optimization problem is formulated, and boundedness conditions of the $\mathscr{L}_1$-norm for the adaptive controller are derived. The theoretical results are illustrated in the fourth section by a case study for the VEGA launch vehicle. The paper ends with some concluding remarks.

Throughout the five chapters, the following notations will be used: $\mathbb{N}$ and $\mathbb{R}$ denote the sets of natural and real numbers, respectively. The 1-norm of a vector. $u \in \mathbb{R}^n$ is written by definition:

$$\|u\|_1 = \sum_{i=1}^{n} |u_i|$$

and its 2-norm is defined as:

$$\|u\|_2 = \sqrt{u^T u}$$

in which 'T' stands for the transpose of the vector (or of a matrix). For a real square matrix $M \in \mathbb{R}^{n\times n}$, the notation $M > 0$ ($M < 0$) means that M is symmetrically positive (negative) definite. Similarly, the notation $M \geq 0$ ($M \leq 0$) means that M Is symmetric positive (negative) semidefinite. By I one denotes the unit matrix of appropriate dimensions, and by $tr(\bullet)$, the trace of the square matrix $(\bullet)$.

2. Preliminaries

Definition 1. Given a stable single-input single-output (SISO) proper linear system with the transfer function $H(s)$, its $\mathscr{L}_1$-norm is defined as:

$$\|H(s)\|_{\mathcal{L}_1} = \int_0^{\infty} |h(t)| dt$$

where $h(t)$ denotes the impulse response of the system. An upper bound of the $\mathscr{L}_1$-norm is given by the following result, whose proof may be found in [16, 17].

Theorem 1. Consider the SISO stable proper system H with the state space realization:

$$\begin{aligned} \dot{x}(t) &= Ax(t) + Bu(t) \\ y(t) &= Cx(t)\ . \end{aligned} \tag{1}$$

Then, if the matrix inequality:

$$AP_\alpha + P_\alpha A^T + \alpha P_\alpha + \frac{1}{\alpha} BB^T \leq 0 \tag{2}$$

has a positive definite solution $P_\alpha > 0$ for a certain $\alpha > 0$, then,

$$\|H(s)\|_{\mathcal{L}_1} \leq \|CP_\alpha C^T\|_2. \tag{3}$$

in which, by definition,

$$\|CP_\alpha C^T\|_2 = tr^{\frac{1}{2}}(CP_\alpha C^T).$$

Remark 1. It is known that Eq. (2) may be conservative [18]. In [16], the authors introduced the so-called $*$-norm defined as:

$$\|H\|_* := \inf_\alpha \|CP_\alpha C^T\|_2,$$

suggesting that in many engineering applications, this norm is a relatively tight upper bound of the above-defined $\mathscr{L}_1$-norm.

3. Problem Formulation and Boundedness Conditions for the $\mathscr{L}_1$-Norm

Consider the following class of SISO linear systems:

$$\begin{aligned} \dot{x}(t) &= Ax(t) + B\big(u(t) + \theta x(t)\big) \\ y(t) &= Cx(t) \end{aligned} \tag{4}$$

where $x \in \mathbb{R}^n$ denotes the state vector, $u \in \mathbb{R}$ is the control variable, $y \in \mathbb{R}$ stands for the measured output and $\theta \in \mathbb{R}^{1\times n}$ is a vector including unknown bounded parametric modeling uncertainties.

Given the ideal model with the Hurwitz state matrix A_m, the purpose of the $\mathscr{L}_1$ adaptive control design developed in [15] is to ensure that the output $y(t)$ tracks a reference signal $r(t)$ for all values of the uncertain parameter vector θ. It is proven that if it exists a SISO stable filter $C_f(s)$ with $C_f(0) = 1$, such that:

$$\|G(s)\|_{\mathcal{L}_1} \leq \frac{1}{L}, \tag{5}$$

where

$$G(s) := H(s)\left(1 - C_f(s)\right)$$

in which,

$$H(s) := C(sI - A_m)^{-1}B$$

then the $\mathscr{L}_1$ adaptive controller derived in [15] ensures the stability of the closed-loop system for all uncertain parameters θ with $\|\theta\|_1 < L$.

It follows that, to maximize the robustness radius L, one may design a stable proper filter $G_f(s)$ for which $\|G(s)\|_{\mathcal{L}_1}$ is minimized. In [15], the design of this filter is performed for particular orders and structures containing a single parameter. This parameter is then determined using a direct searching approach.

In the present paper, a different method is presented. It considers the general form of the proper filter with the transfer function $C_f(s)$ and with the state-space representation:

$$\begin{aligned} \dot{x}_c(t) &= A_c x_c(t) + B_c u_c(t) \\ y_c(t) &= C_c x_c(t) \end{aligned} \tag{6}$$

in which the state matrix $A_c \in \mathbb{R}^{n_c \times n_c}$ with fixed order $n_c \in \mathbb{N}$ is Hurwitz, together with the condition $C_f(0) = 1$, namely,

$$-C_c {A_c}^{-1} B_c = 1. \tag{7}$$

Based on the representation (6) with the constraint (7) of the filters $C_f(s)$ and taking into account the condition (5), the aim is to minimize $\|G(s)\|_{\mathcal{L}_1}$, maximizing thus the robustness radius L.

If the system $H(s)$ has the state space equations:

$$\begin{aligned} \dot{x}_m(t) &= A_m x_m(t) + B u_m(t) \\ y_m(t) &= C x_m(t), \end{aligned}$$

direct computations based on the representation (6) show that the system with the transfer function:

$$G(s) := H(s)\left(1 - C_f(s)\right)$$

has the state space equations

$$\begin{aligned} \dot{x}_g(t) &= \mathcal{A} x_g(t) + \mathcal{B} u(t) \\ y(t) &= \mathcal{C} x_g(t), \end{aligned} \tag{8}$$

where,

$$x_g := [{x_m}^T \quad {x_c}^T]^T$$

in which,

$$\mathcal{A} := \begin{bmatrix} A_m & -BC_c \\ 0 & A_c \end{bmatrix}, \quad \mathcal{B} := \begin{bmatrix} B \\ B_c \end{bmatrix}, \quad \mathcal{C} := [I \quad 0].$$

Applying Theorem 1 for the system (8), it results that if there exists an $\alpha > 0$ and $P_\alpha > 0$ and such that:

$$\mathcal{A} P_\alpha + P_\alpha \mathcal{A}^T + \alpha P_\alpha + \frac{1}{\alpha} \mathcal{B}\mathcal{B}^T \leq 0 \tag{9}$$

then,

$$\|G(s)\|_{\mathcal{L}_1} \leq \|\mathcal{C} P_\alpha \mathcal{C}^T\|_2.$$

For the partition of P_α conformably with one of $\mathcal{A}$,

$$P_\alpha = \begin{bmatrix} P_1 & P_2 \\ {P_2}^T & P_3 \end{bmatrix}$$

condition (9) leads to:

$$\begin{bmatrix} A_m P_1 + P_1 {A_m}^T - BC_c {P_2}^T - P_2 {C_c}^T B^T + \alpha P_1 & A_m P_2 - BC_c + P_2 {A_c}^T + \alpha P_2 & B \\ \left(A_m P_2 - BC_c + P_2 {A_c}^T + \alpha P_2\right)^T & A_c P_3 + P_3 {A_3}^T + \alpha P_3 & B_c \\ B^T & {B_c}^T & -\alpha \end{bmatrix} \leq 0 \tag{10}$$

Since, $C := [I\ 0]$ using the above partition of P, it results that $\mathcal{C} P_\alpha \mathcal{C}^T = P_1$. It follows that to determine A_c, B_c and C_c, one may solve the following optimization problem:

$$\min tr(P_1), \tag{11}$$

subject to the constraints (10) and (7). On the other hand, condition (7) may be rewritten as:

$$C_c w + 1 = 0 \tag{12}$$

with $w \in \mathbb{R}^{n_c}$ satisfying the following conditions:

$$A_c w = B_c. \tag{13}$$

The optimization problem (11) with the constraints (10), (12), (13), and $P_\alpha > 0$ is bilinear with respect to the unknown variables $A_c, B_c, C_c, P_1, P_2, P_3, w$ and $\alpha > 0$. Although such problems are not convex, they may efficiently be solved numerically using specialized software packages recently developed, among which one mentions [19, 20].

4. Mathematical Models of the Launch Vehicle Pitch/Yaw Dynamics and of the TVC Actuator

In this section, one presents the design models and approximations for the launch vehicle and for the TVC actuator. They include the linearized models for the pitch/yaw dynamics in the case when the launcher is considered a rigid body, and the flexible modes representation [21], and finally, the TVC actuator dynamics.

4.1. Launch vehicle model

Figure 1(a) shows the rigid body dynamic model for the pitch motion diagram, and Fig. 1(b) shows the scheme of the adaptive control system, in which θ denotes the pitch angle, $\dot{z}$ is the lateral drift speed, α stands for the angle of attack, α_w is the wind incidence, m is the vehicle mass, V is the launcher velocity, T is the thrust, D is the drag, L_α is the aerodynamic force acting on the center of pressure, ℓ_{CG} is the swivel point C and the center of gravity G, I_{yy} is the pitch moment of inertia, δ is the gimbal deflection angle, ℓ_{GA} is the distance from the center of gravity to the aerodynamic center of pressure, C_N is the coefficient of z-aerodynamic force.

Then the following equations for the pitch motion of the vehicle can be obtained (see e.g. [8, 12, 21, 22, 28]):

$$\ddot{\theta} = a_6\alpha - k_1 \sin(\delta) \tag{14}$$

where the parameters a_6 and k_1 are defined in Eq. (19).

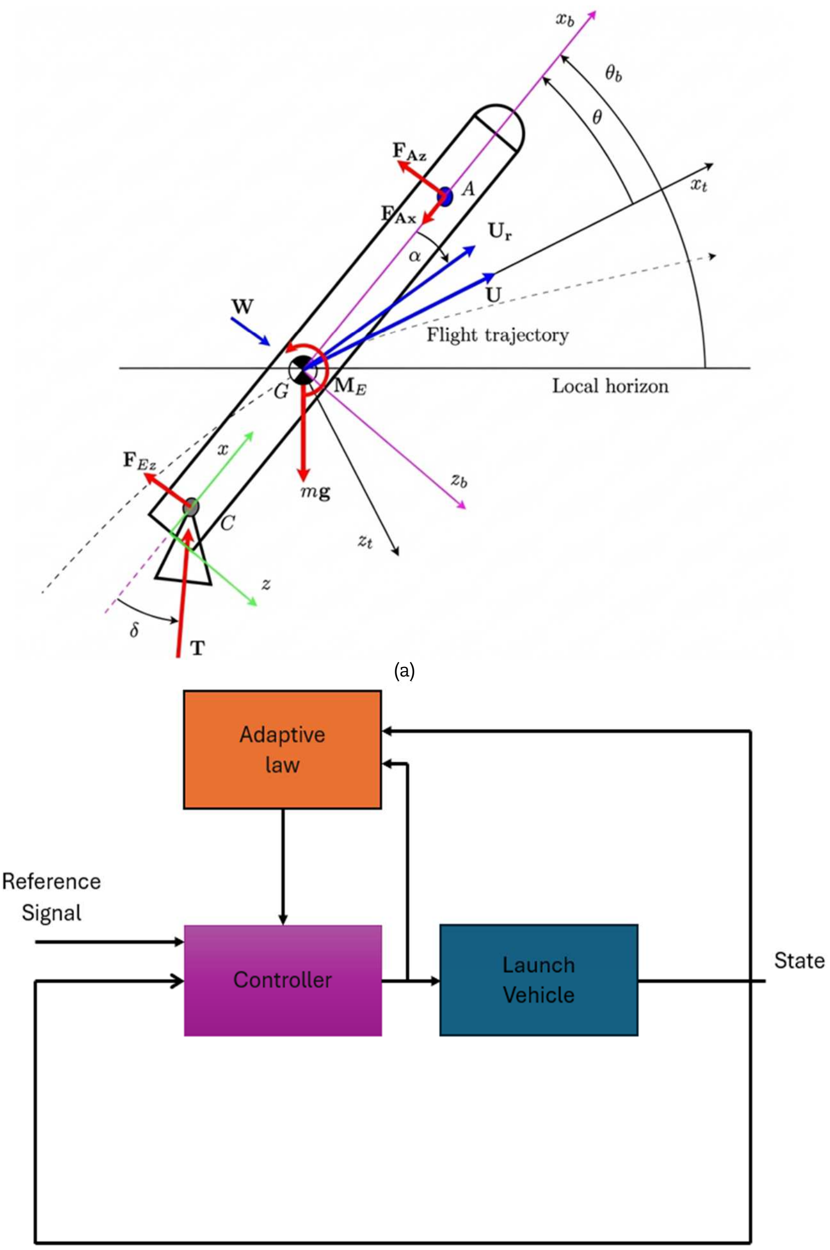

Fig. 1. The rigid body dynamic pitch: (a) Motion diagram [21], (b) scheme of the adaptive control system.

However, this model was built assuming that there was no drift and no wind, so working with small angles and accepting that $\alpha = \theta$, the equation can also be rewritten as:

$$\ddot{\theta} = a_6\theta \ - k_1 \sin(\delta). \tag{15}$$

Considering the wind incidence α_w acting as a perturbation on the pitch dynamics, one can express the angle of attack as:

$$\alpha = \theta + \frac{\dot{z}}{V} - \alpha_w \tag{16}$$

where $\dot{z}$ denotes the lateral drift speed. Due to this modification, the equations of motion are rewritten for small deflections δ as:

$$\begin{aligned} \ddot{\theta} &= a_6\alpha - k_1\delta \\ \ddot{z} &= -\tfrac{L_\alpha}{m}\alpha - \tfrac{T}{m}\delta - \tfrac{T-D}{m}\theta. \end{aligned} \tag{17}$$

From Eq. (17), it results that the linearized model of the pitch motion has the following state-space representation:

$$\begin{bmatrix} \dot{\theta} \\ \ddot{\theta} \\ \ddot{z} \end{bmatrix} = \begin{bmatrix} 0 & 1 & 0 \\ a_6 & 0 & \dfrac{a_6}{V} \\ -a_1 & 0 & -a_2 \end{bmatrix} \begin{bmatrix} \theta \\ \dot{\theta} \\ \dot{z} \end{bmatrix} + \begin{bmatrix} 0 & 0 \\ a_6 & -k_1 \\ a_6 \ .\mathrm{V} & -a_3 \end{bmatrix} \begin{bmatrix} \alpha_w \\ \delta \end{bmatrix} \tag{18}$$

in which the model parameters have the following expressions [8, 12, 21]:

$$a_1 = \tfrac{L_\alpha + T - D}{m}, \quad a_2 = \tfrac{L_\alpha}{mv}, \quad a_3 = \tfrac{T}{m}, \tag{19}$$

$$a_6 = \tfrac{L_\alpha \ell_{GA}}{I_{yy}}, \ L_\alpha = qSC_{N_\alpha}, \ k_1 = \tfrac{T\ell_{CG}}{I_{yy}}. \tag{20}$$

One mentions that the linearized system with Eq. (18), modelling the launcher pitch/yaw motion, is inherently unstable at any flight condition. Therefore, a stabilization control system is required to maintain the vehicle on the desired flight trajectory.

Moreover, the linearized model in Eq. (18) is derived under the assumption that the vehicle is a rigid body. For a slender launcher, structural deformations introduce bending modes [22, 23], getting worse the stability performances of the control system. The total pitch deflection θ becomes in this case:

$$\theta = \theta_r + \sum_{i=1}^{n} \phi_i \, q_i. \tag{21}$$

The dynamics of the launch vehicle considering the effects of the flexible modes is represented as:

$$H_l(s) = H_{rigid}(s) + H_{flex}(s)$$

where $H_{rigid}(s)$ denotes the transfer function corresponding to the linearized rigid body model of the launcher and $H_{flex}(s) = \sum_{j=1}^{3} H_j(s)$ from [24] with:

$$H_j(s) = \frac{k_j}{s^2 + 2\zeta_j \omega_{n_j} s + {\omega_{n_j}}^2} \tag{22}$$

j = 1, 2, 3, representing the elastic mode index, with k_j, ζ_j and ω_{n_j}, standing for the gain, damping coefficient, and the natural frequency of the flexible mode j, respectively. For the numerical example presented in Section 6, the following numerical values have been considered, corresponding to a payload of 1200 kg: k = 7.07, ω_{n1} = 24.66 rad/s, ω_{n2} = 53.93 rad/s and ω_{n3} = 74.15 rad/s.

5. $\mathscr{L}_1$ Adaptive Controller Structure

In the present paper, an $\mathscr{L}_1$ control configuration with model reference adaptive control (MRAC) with a state predictor have been adopted. More details may be found, for instance, in [13, 14, 15, 25, 26, 27].

The state-space model is expressed as:

$$\dot{x} = Ax + Bu + f(x,t) \tag{23}$$

where, $x = \left[\theta, \dot{\theta}, \dot{z}\right]^T$, $u = \delta$ and the nonlinear $f(x,t)$ is continuous and bounded, incorporating the unmodeled dynamics and nonlinearities of the motion dynamics.

The linear part of Eq. (23), $\dot{x} = Ax + Bu$, is given in Eq. (18). The $\mathscr{L}_1$-norm minimization adaptive control methodology requires performing a pre-stabilization of the linear part in Eq. (23) using a state-feedback control law of the form $u_m(t) = -k_m x(t)$ such that the state matrix $A_m = A - Bk_m$ is Hurwitz. In the present paper, for the considered case study presented in Section 6, the vector k_m includes the gains corresponding to a PD (Proportional-Derivative) linear controller designed for the linearized model corresponding to the maximal dynamic pressure. Then, the adaptive control law is expressed as a sum of $u_m(t)$ and a nonlinear adaptive component. This component is obtained using a state-predictor and a projection-type adaptive law. The nonlinear stability of the resulting system is proved in Chapters 2 and 3 of [15] based on Lyapunov-type arguments. The block diagram of the control system of the closed-loop model reference adaptive control architecture with a state predictor is presented in Fig. 2.

6. $\mathscr{L}_1$ Adaptive Control for the VEGA Launch Vehicle

In this section, we will present the behavior of the control input δ, and we will explain the $\mathscr{L}_1$ adaptive control with a rigid launch vehicle when we use the filter $C_f(s)$, and we will show how $\mathscr{L}_1$ adaptive control deals with the flexible launch vehicle in the case of using a filter $C_f(s)$ at payload 1200 kg, and how behave the aerodynamic load versus Mach number with $\mathscr{L}_1$ adaptive controller, and we will clarify by plots the responses of the Vega Launch vehicle after optimizing the limit of the robustness.

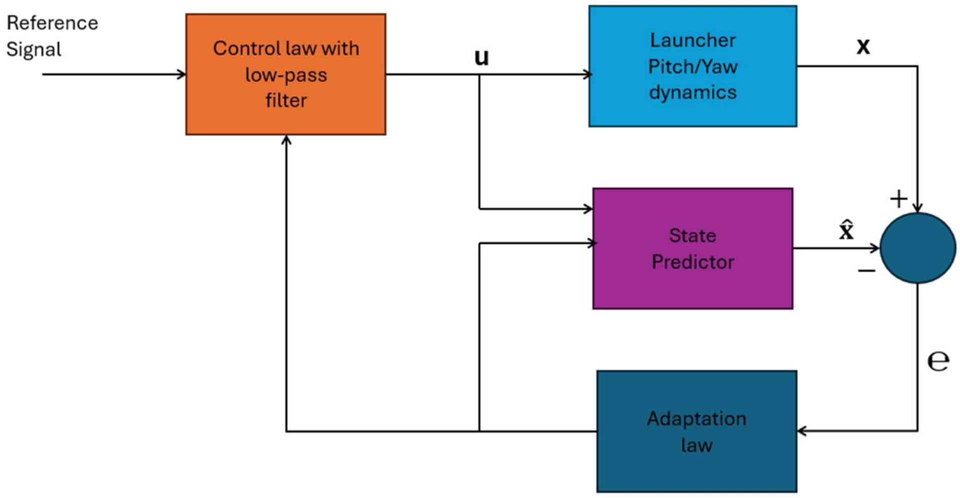

Fig. 2. Closed- loop model reference adaptive control architecture with state-predictor [15].

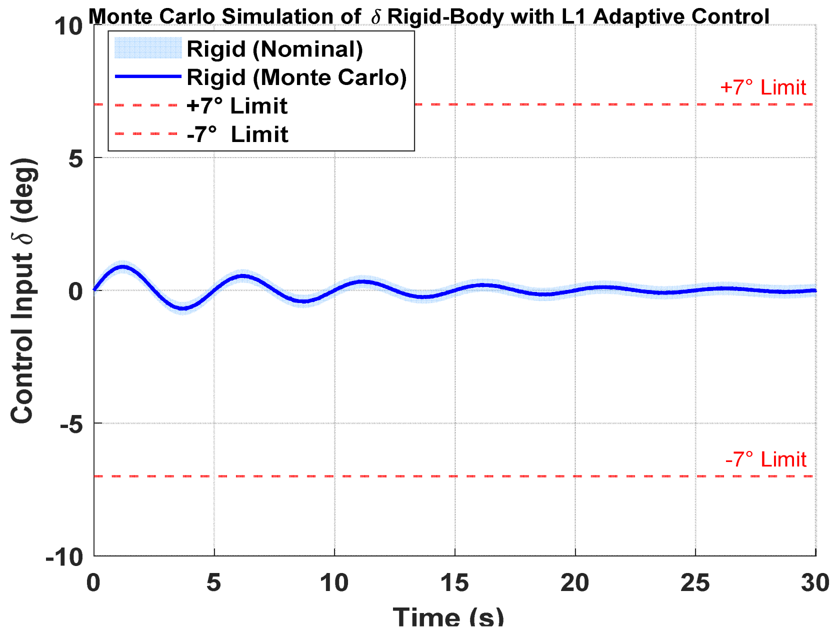

Fig. 3. The Rigid Configuration of the control signal behavior $\delta(t)$ for the rigid body.

6.1. Control input time response

The control input signal $\delta(t)$ has been analyzed when we use the $\mathscr{L}_1$ adaptive controller. In Fig. 3, we observe the behavior of the control input signal, showing both the nominal response and the Monte Carlo simulation responses under the $\mathscr{L}_1$ adaptive controller. We see that the control input does not exhibit high-frequency oscillations. The signal remains smooth, well within the operational limits of ±7°, and demonstrates stable transient and steady-state behavior without any abrupt.

6.2. $\mathscr{L}_1$ adaptive control with a rigid launch vehicle and filter $C_f(s)$

Figure 2 shows the block diagram of the rigid launch vehicle with the actuator and delay τ = 0.015 sec, filter $C_f(s)$, ω_c = 30 rad/s, α_w = 0.025 rad, reference signal r = 0.1 rad. After simulating using the configuration from this block diagram, we obtained the responses of theta, alpha, and lateral velocity, as shown in Fig. 4.

Figure 4(a) presents the responses of the pitch angle $\theta(t)$ when this rocket is used for a payload of 1200 kg with the rigid model of the launch vehicle. The pitch angle stabilizes with amplitude 0.1 rad at a short time 10 seconds, Fig. 4(b) presents the time responses of alpha, the oscillations decay over time, showing the system's ability to reduce instability and suppress high-frequency oscillations, and there is the slow drift, which instead of settling to zero, α gradually decreases, indicating a long-term trend, possibly due to payload-induced effects or external disturbances. The slow drift in α might indicate payload influence, actuator limitations, or slight model mismatches. As shown in Fig. 4(c), the velocity continues to decrease, reaching around -80 m/s at 30 seconds. This indicates that the launch vehicle is being driven laterally due to the combination of wind disturbance and the control system trying to correct it. The smooth response suggests that $\mathscr{L}_1$ control is successfully mitigating large deviations while allowing gradual adaptation. The lateral velocity response confirms that the $\mathscr{L}_1$ adaptive control effectively stabilizes the launch vehicle despite wind disturbances and control delays. The initial small oscillations are quickly damped, and the vehicle follows a smoothly decreasing trajectory, which indicates a controlled lateral drift due to external factors like wind and thrust vectoring. The system is robust, and the control strategy ensures that lateral deviations do not grow uncontrollably, maintaining stability and adaptability.

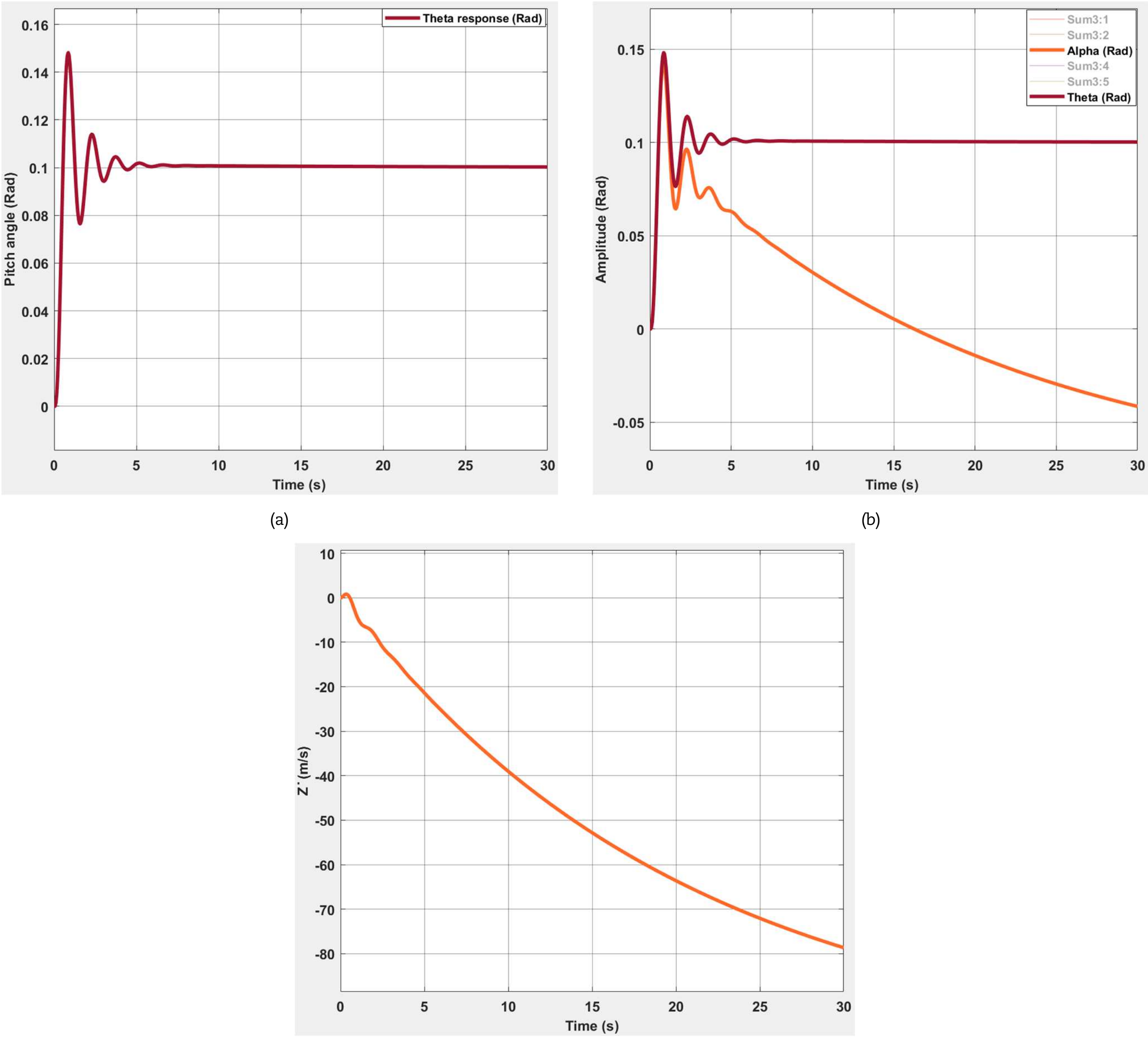

(a) (b) (c)

Fig. 4. Response of the rigid launch vehicle with $\mathscr{L}_1$ adaptive control, with a filter $C_f(s)$, at $\omega_c = 47(rad/sec)$, $\alpha_w = 0.08\ rad$, $r - reference = 0.1\ rad$, delay $\tau = 0.015\ sec$ in case of: (a) Time responses of the pitch angle $\theta(t)$, (b) Time responses of the pitch angle $\theta(t)$ and alpha, (c) Time response of the lateral drift velocity.

6.3. $\mathscr{L}_1$ adaptive control with flexible launch vehicle and filter $C_f(s)$ at payload 1200 kg

The $\mathscr{L}_1$ adaptive controller design methodology is presented in [15]. It aims to enhance robust properties for fast adaptation. This is why some aviation applications have been previously developed in papers like [15, 26, 27]. The theoretical solution proposed in [15] includes in the adaptive architecture some low-pass filters $C_f(s)$ subject to the condition $C_f(0) = 1$. It is proven that if $\left\|H(s)\left(1 - C_f(s)\right)\right\|_{\mathcal{L}_1} < \frac{1}{L}$ with $H(s)$ corresponding to the reference model, then robust stability of the closed-loop system is guaranteed for all parameters θ of the controlled plant satisfying the condition $\|\theta\|_1 < L$. Based on these theoretical developments, an $\mathscr{L}_1$ adaptive control law for the TVC system of the European Vega launcher is presented in Fig. 2, which explains the block diagram of the Vega launcher using the $\mathscr{L}_1$ adaptive controller with the addition of a Butterworth filter introduced to attenuate the effect of the flexible modes with a payload of 1200 kg. One added to the configuration of the $\mathscr{L}_1$ adaptive controller filter $C_f(s)$ in order to reduce the disturbance effect and to improve the robustness of the closed-loop system with respect to parametric uncertainties, the first-order filter with the transfer function $C_f(s) = \frac{\omega_c}{s+\omega_c}$. The next stage in applying the $C_f(s)$ adaptive controller consists of minimizing the $\mathscr{L}_1$-norm of $H(s)\left(1 - C_f(s)\right)$ for filter $C_f(s)$. For the minimization of the $\mathscr{L}_1$-norm, one may use, for instance, the results presented in Appendix C of [15] requiring the solution of a specific system of linear matrix inequalities (LMIs). Since this method can provide conservative results, an alternative solution can be obtained using the numerical procedure given in [6] based on the theoretical results derived in [2]. Applying this latest procedure, one found that for $\omega_c = 47\frac{\text{rad}}{\text{sec}}$, the condition $\left\|H(s)\left(1 - C_f(s)\right)\right\|_{\mathcal{L}_1} < \frac{1}{L}$ is fulfilled (see Fig. 5(a)). Figure 5(b) presents the time responses of the pitch angle $\theta(t)$. The red plot was obtained without the Butterworth filter, while the blue plot shows the time response of the pitch angle with the Butterworth filter, for a commanded value of theta of 0.8 rad. Thus, it is shown that the pitch angle response for the system with the Butterworth filter reduces high-frequency components while maintaining the system's stability.

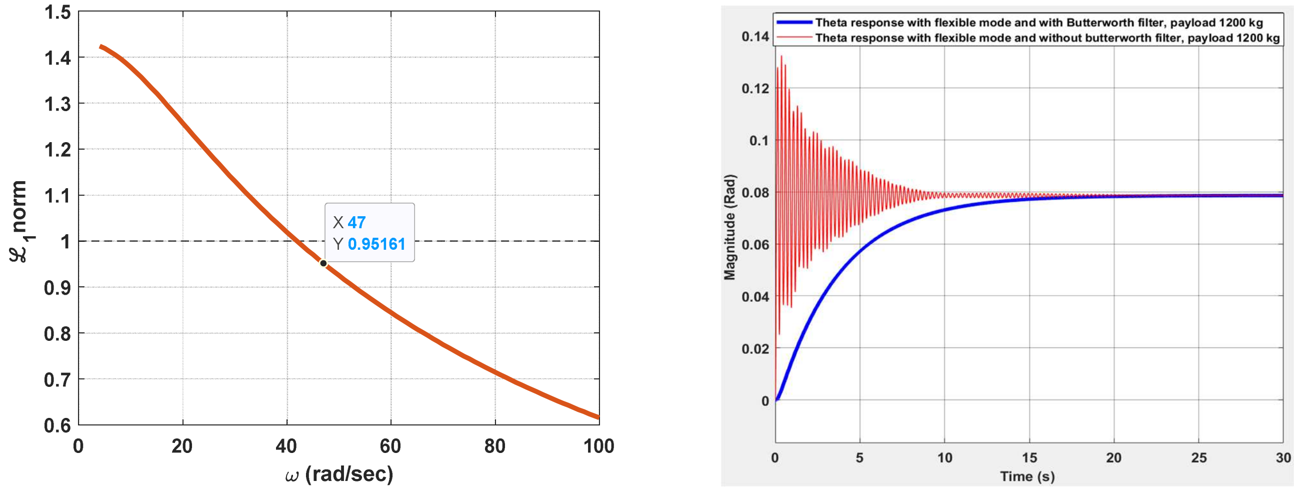

(a) (b)

Fig. 5. The $\mathscr{L}_1$ adaptive control, with Filter C_f(s), $\omega_c = 47(rad/sec)$, $\alpha_w = 0.08\ rad$, $r - reference = 0.1\ rad$: (a) $\mathscr{L}_1$norm, (b) Theta response with the Butterworth filter and the flexible mode.

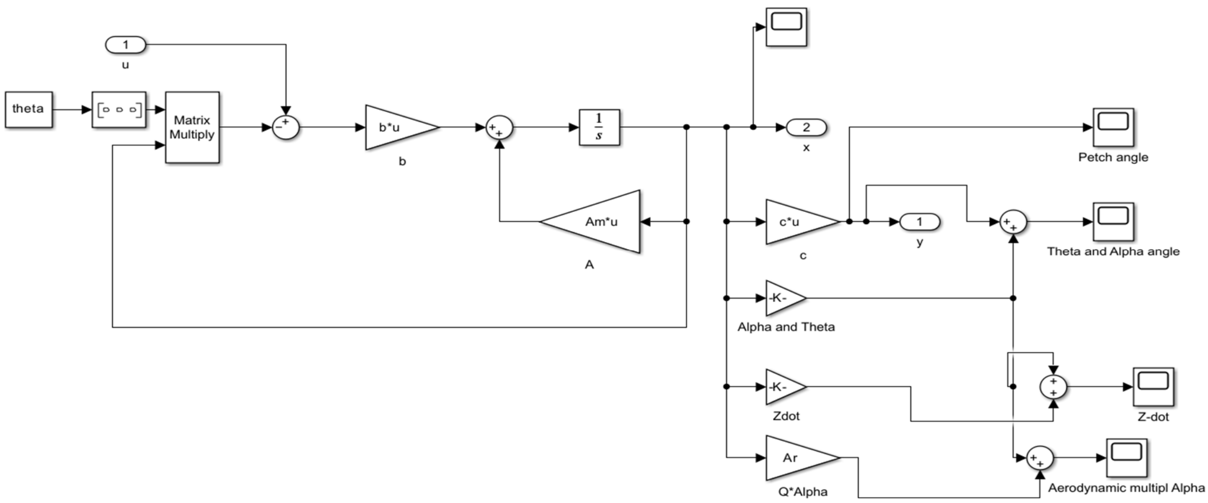

Fig. 6. The block diagram responses of the launch vehicle with a payload of 1200 kg.

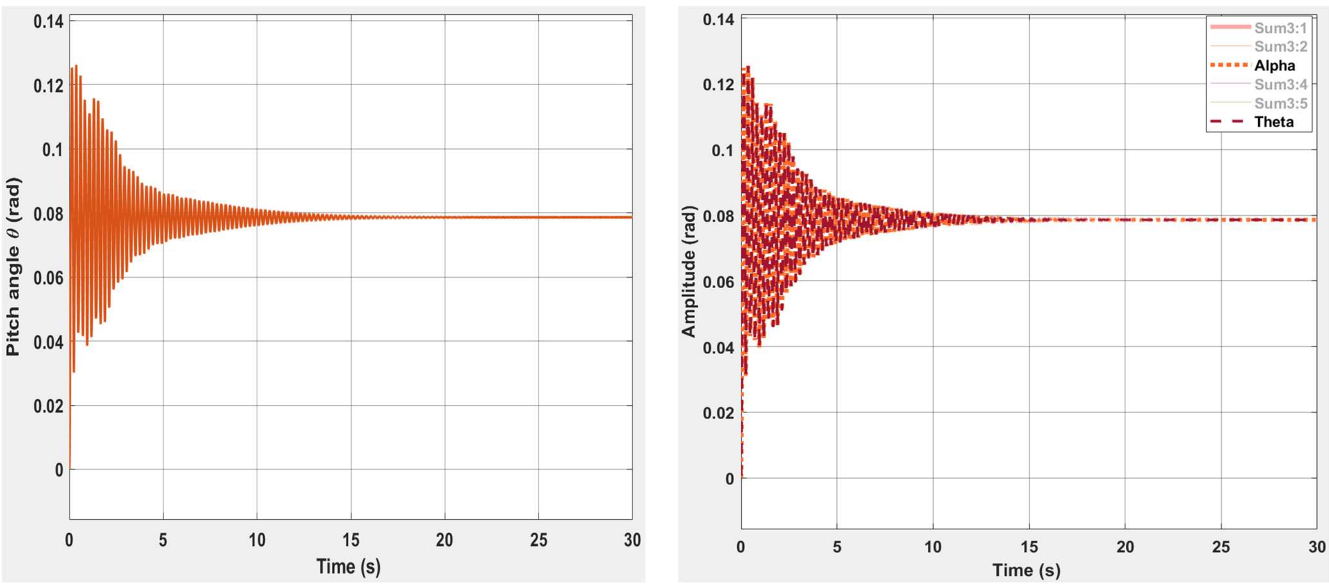

(a) (b)

Fig. 7. The Time responses of the $\mathscr{L}_1$ adaptive control with a Butterworth filter at flexible mode, with filter $C_f(s)$, $\omega_c = 47(rad/sec)$, $\alpha_w = 0.08\ rad$, $r - reference = 0.1\ rad$ in case of: (a) The pitch angle $\theta(t)$, (b) The pitch angle $\theta(t)$ and $\alpha(t)$.

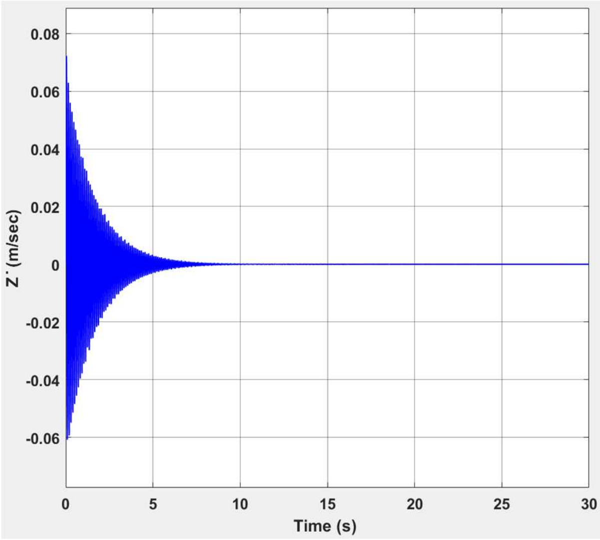

Fig. 8. The lateral drift velocity with a Butterworth filter at flexible mode with $\mathscr{L}_1$ adaptive control, with Filter $C_f\,(s)$, $\omega_c = 47(rad/sec)$, $\alpha_w = 0.08\ rad$, $r - reference = 0.1\ rad$.

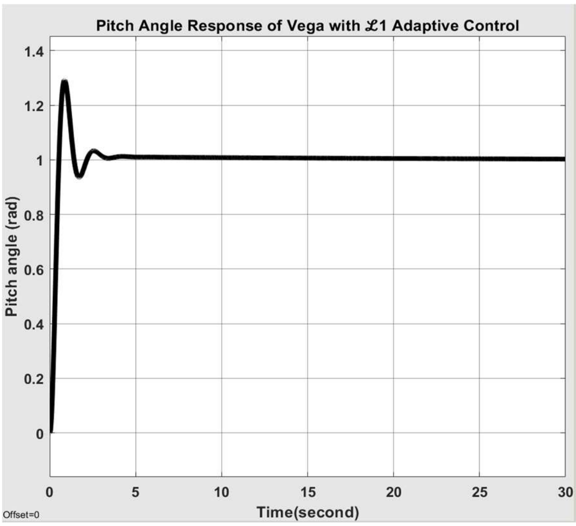

Fig. 9. Theta response for a rigid body Vega.

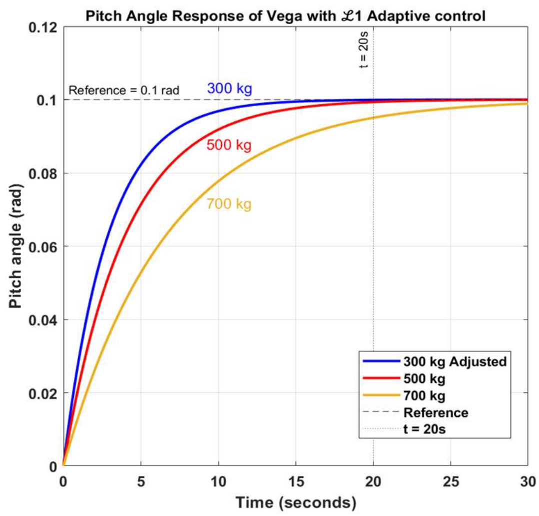

Fig. 10. Theta response of a flexible body Vega with a Butterworth filter.

Further, using the configuration in Fig. 6 presents the block diagram of the flexible launch vehicle of the time responses theta, alpha, and the lateral velocity when this rocket is used for a payload of 1200 kg (see Fig. 6).

Figures 7(a) and 7(b) show the responses of theta and alpha when this rocket is used for a payload of 1200 kg with the flexible launch vehicle. It presents the responses of the pitch angle $\theta(t)$ and $\alpha(t)$ for a commanded theta value of 0.8 rad. This demonstrates that the pitch angle response for the system containing the Butterworth filter reduces high-frequency components while maintaining the system's stability.

Figure 8 shows the lateral velocity responses when this rocket is used for a 1200 kg payload with the flexible launch vehicle. The lateral velocity response ranges from 0.06 m/sec to -0.06 m/sec, and by 10 seconds, it stabilizes at 0 m/sec.

6.4. Comparing numerical results with the $\mathscr{L}_1$ adaptive controller

By using the same parameters that were used in [21], we have obtained a better performance with the $\mathscr{L}_1$ adaptive controller in Figs. 9 and 10 than with the Proportional-Derivative (PD) controller in Fig. 11, as shown in the figures.

Figure 9 shows the theta response for the rigid body with the $\mathscr{L}_1$ adaptive controller [28]. In contrast, Fig. 10 shows the theta response of the flexible body with three payloads with the $\mathscr{L}_1$ adaptive controller is down [29]. In Fig. 11, the theta response with the PD classical controller.

Analyzing the system's behavior using both the classical PD controller used in [21], as shown in Fig. 11, and the $\mathscr{L}_1$ adaptive controller used in this paper, as shown in Figs. 9 and 10, clearly indicates that the $\mathscr{L}_1$ controller offers superior robustness, faster settling time, reduced overshoot, and greater stability margins. The figures illustrate that the classical controller struggles to handle significant parameter changes, often pushing the system to the edge of instability. In contrast, the $\mathscr{L}_1$ adaptive controller maintains stability and delivers consistent, reliable performance. The best outcome for the $\mathscr{L}_1$ controller occurs under nominal parameter values, whereas the PD controller performs best when parameters are reduced by 20%. This comparison supports the conclusion that the $\mathscr{L}_1$ adaptive controller outperforms the classical controller in terms of overall system performance. The PD controller obtained in [21] typically yields conservative but reliable margins for the assumed uncertainty range; it does not change online, so its performance under parameter excursions outside the modeled set can be poor, and in contrast the $\mathscr{L}_1$ provides uniform, guaranteed transient and steady-state bounds (under the $\mathscr{L}_1$-norm condition) and can maintain tracking and stability under fast, significant parameter changes that would require frequent re-scheduling in a fixed controller.

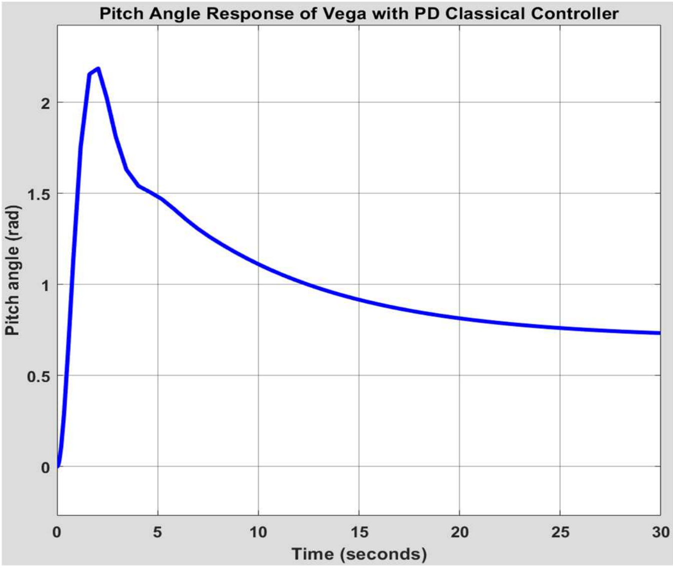

Fig. 11. Theta response with the PD classical controller.

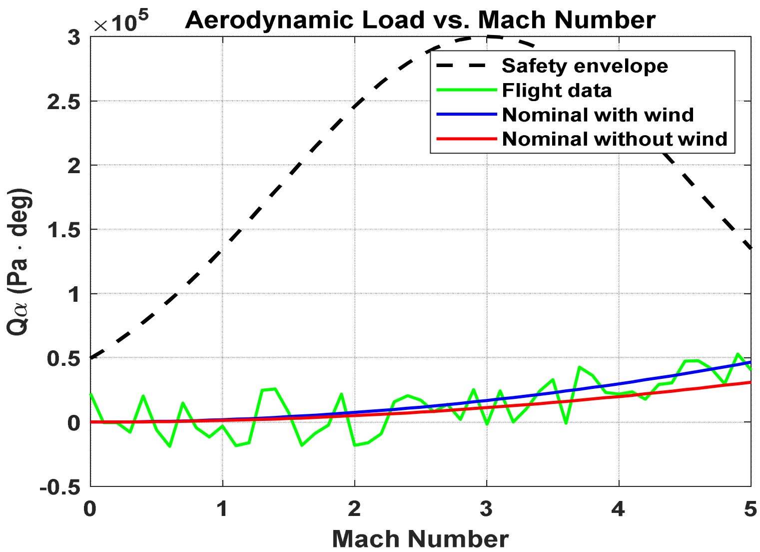

Fig. 12. The aerodynamic load versus the Mach number, at $\omega_c = 30\ (rad/sec)$, $\alpha_w = 0.025\ rad$, and $r - reference = 0.1\ rad$, delay $\tau = 0.015\ sec$, and $\alpha = 0.135\ rad$.

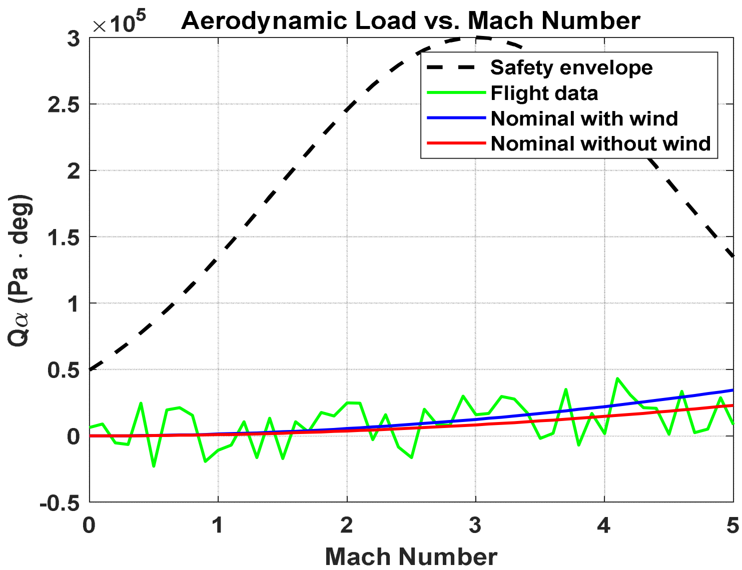

Fig. 13. The aerodynamic load versus the Mach number at $\omega_c = 47\ rad/sec$, $\alpha_w = 0.08\ rad$, and $r - reference = 0.1\ rad$, and $\alpha = 0.1\ rad$.

6.5. $\mathscr{L}_1$ adaptive controller with aerodynamic load versus Mach number

The wind plays a critical role in the overall trend in terms of aerodynamic load; thus, every worst-case scenario is wind-dependent [9]. An analysis of the aerodynamic load is performed by determining the product $Q\alpha$ where $Q = \frac{1}{2}\rho v$ denotes the dynamic pressure, depending on the air density ρ and on the vehicle's speed, v and where α is its angle of attack.

6.5.1. *Aerodynamic load vs. Mach number at the rigid launch vehicle with actuator and delay*

The aerodynamic load versus the Mach number is represented in Fig. 12 together with the upper safety limit in the case when the filter $C_f(s)$ is used in the $\mathscr{L}_1$ adaptive controller configuration at the rigid launch vehicle, at $\omega_c = 30\ rad/sec$, $\alpha_w = 0.25\ rad$, and $r - reference = 0.1\ rad$, delay $\tau = 0.015\ sec$, and $\alpha = 0.135\ rad$.

From Fig. 12 of the aerodynamic load versus Mach number for the rigid launch vehicle, we conclude that the system remains within tolerable limits, allowing the structure to withstand aerodynamic forces. We see from the figure that flight data points that fall inside the envelope indicate safe operation. We see that the curve for nominal with wind typically lies above the curve for nominal without wind, indicating the additional load caused by environmental factors.

6.5.2. *Aerodynamic load versus Mach number at the flexible launch vehicle*

Figure 13 represents the aerodynamic load versus the Mach number, which is represented together with the upper safety limit in the case when the filter $C_f(s)$ is used in the $\mathscr{L}_1$ adaptive controller configuration at the flexible launch vehicle, at $\omega_c = 47\ rad/sec$, $\alpha_w = 0.08\ rad$, and $r - reference = 0.1\ rad$, and $\alpha = 0.1\ rad$.

From Fig. 13 of the aerodynamic load versus Mach number for the flexible launch vehicle, we notice that the system remains within tolerable limits, allowing the structure to withstand aerodynamic forces. We see from the figure that flight data points that fall inside the envelope indicate safe operation. We see that the curve for nominal with wind typically lies above the curve for nominal without wind, indicating the additional load caused by environmental factors.

7. The Responses of the Vega Launch Vehicle after Optimizing the Limit of the Robustness

As we mentioned in the introduction, optimizing the parameters of the filter $C_f(s)$ to maximize the robustness radius of the uncertain parameters of the launcher's dynamics requires the $\mathscr{L}_1$-norm of the expression $\|G(s)\|_{L_1} L$ be less than one, in other words, we need to find a stable $C_f(s)$ minimizing $\|G(s)\|_{L_1}$ and $C_f(s) = c(s+a)^{-1}b$, that $a > 0$, and $C_f(0) = 1$, satisfying the condition, which is that c is the output matrix and a is an unknown parameter, but if we try for a long time to transform the nonlinear inequality into a linear inequality in $\|G(s)\|_{L_1}$. The above equations led to minimizing the $\mathscr{L}_1$-norm and the relationship between the function of inequalities $G(s)$ and the transfer function $H(s)$ with the filter $C_f(s)$ and with the robustness (radius inverse proportionality). So, we shall run a numerical simulation to generate plots (optimized pitch angle, angle of attack, and lateral velocity) with the two cases of flexible and rigid launch vehicles using the given parameters. Figure 15 shows the tracking performance of the $\mathscr{L}_1$ adaptive control on angle of attack (α), pitch angle (θ), lateral velocity ($\dot{z}$), and all values are plotted over a short duration (0 – 2 seconds), demonstrating fast dynamic behavior under small-angle inputs. The tracking behavior of the angle of attack (α) follows the reference α_{ref} almost perfectly within 0.25 sec, while its for Pitch Angle (θ) matches the reference θ_{ref} (s) = 0.1 rad with nearly zero steady-state error. The tracking behavior for the lateral velocity starts from 0 and settles near 0.05 m/sec, matching predicted dynamics. Therefore, the $\mathscr{L}_1$ adaptive control demonstrates excellent robustness, stability, and tracking accuracy for the Vega launcher. It ensures that α, θ, and $\dot{z}$ all meet their targets despite delays and uncertainties, making it highly suitable for real-time aerospace applications. The flexible launch vehicle with a payload of 1200 kg, ω_c = 47 rad/sec, α_w =0.08 rad, and r-reference = 0.1 rad (see Fig. 14).

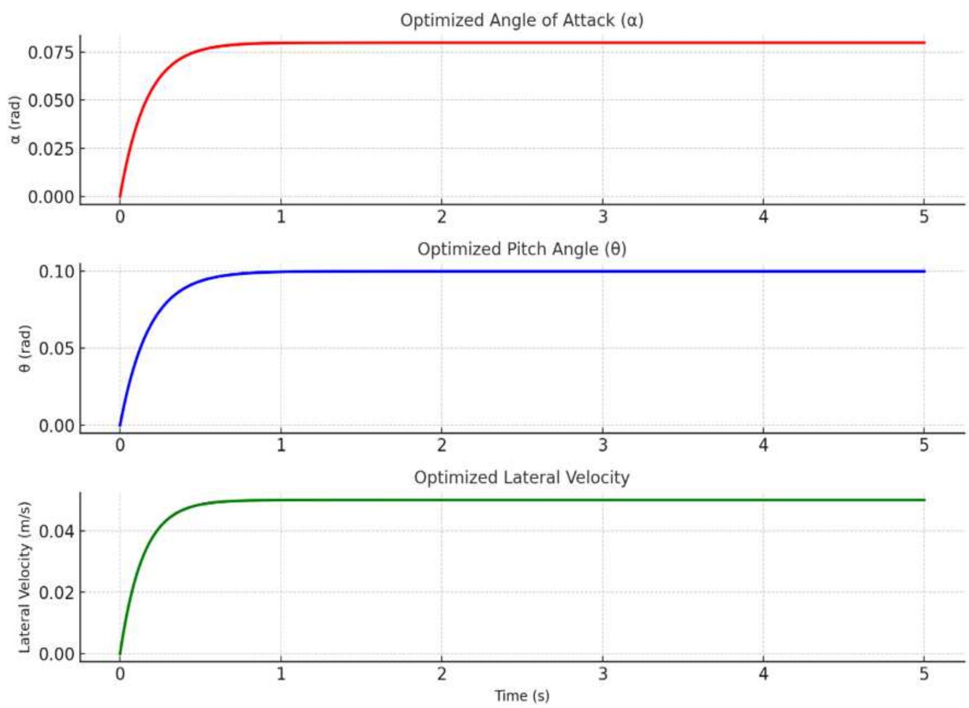

Fig. 14. Optimized pitch angle, angle of attack, and lateral velocity, in the case of a flexible launch vehicle with a payload of 1200 kg at $\omega_c = 47\ (rad/sec)$, $\alpha_w = 0.08\ rad$, and $r - reference = 0.1\ rad$.

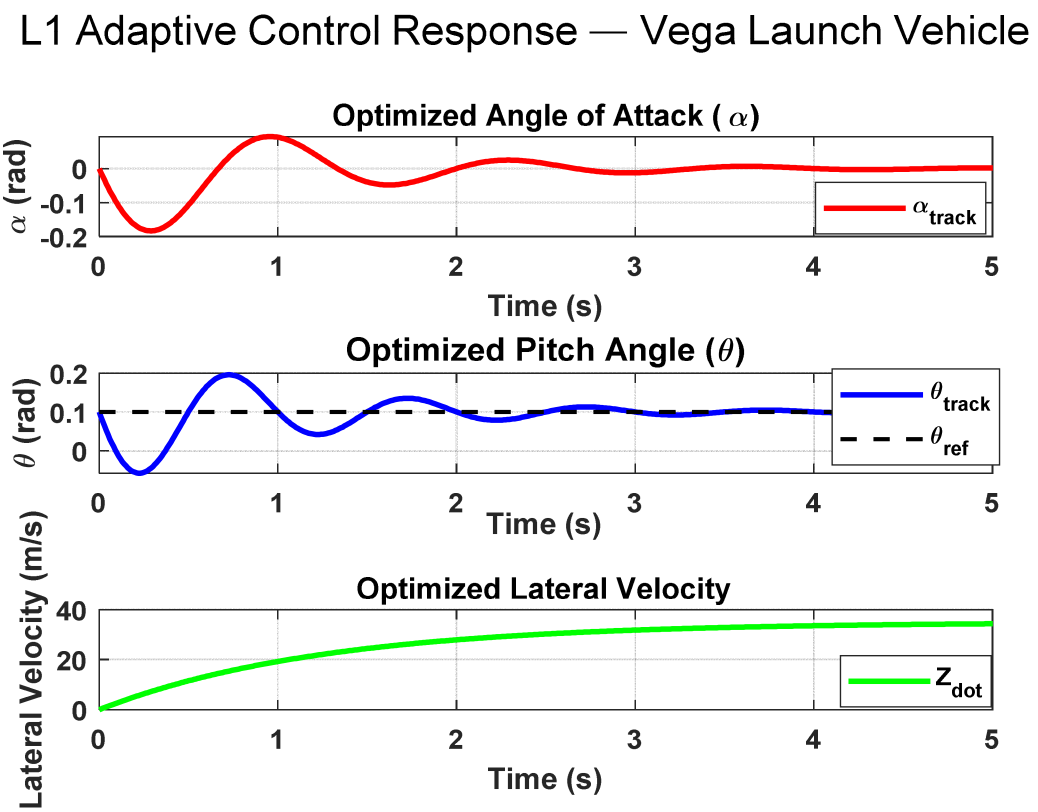

Fig. 15. Optimized pitch angle, angle of attack, and lateral velocity, in the case of a rigid launch vehicle $\omega_c = 30\ (rad/sec)$, $\alpha_w = 0.025\ rad$, and $r-reference = 0.1\ rad$, delay $\tau = 0.015\ sec$.

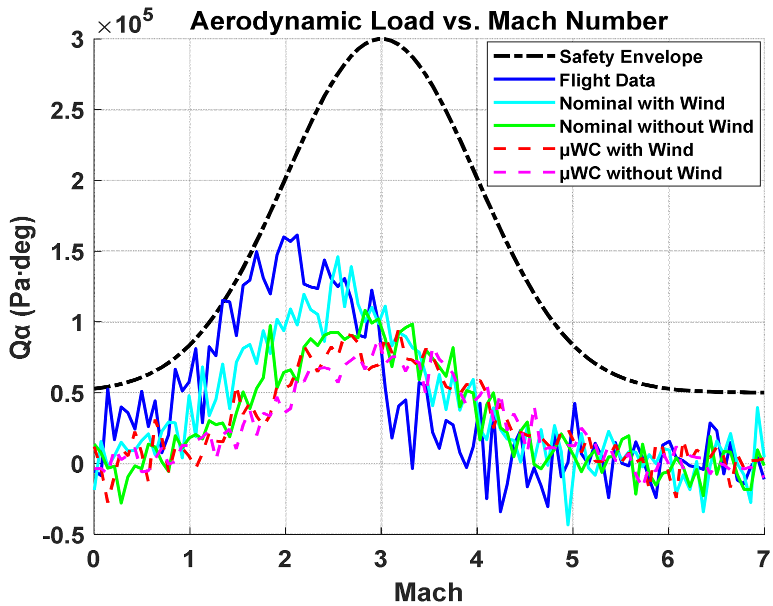

Fig. 16. The aerodynamic load versus the Mach number.

Figure 15 shows the tracking behavior of the angle of attack (α) response, which exhibits underdamped oscillatory behavior at the start but quickly settles within 3 sec. The tracking behavior of the pitch angle (θ) is an oscillatory response with decreasing amplitude and convergence to the reference by $t \approx 4.5$ sec. The response shape of the lateral velocity ($\dot{z}$) is a monotonic growth, a smooth curve without oscillation. The peak value reaches a steady state after about 35-40 m/sec. Therefore, the $\mathscr{L}_1$ adaptive control successfully handles model uncertainties and actuator delay, adapts in real-time to structural flexibility, and preserves boundedness and command-following under dynamic and nonlinear conditions, and the given parameters for the rigid launch vehicle at ω_c = 30 rad/sec, α_w = 0.025 rad, and r-reference = 0.1 rad, delay τ = 0.015 sec (see Fig. 15), while Fig. 16 shows that the $\mathscr{L}_1$ adaptive control ensures safe aerodynamic loads under nominal, windy, and uncertain conditions. The controller adapts dynamically to minimize structural risk while tracking aggressive pitch/α commands. All response curves stay well within the safety envelope, proving the robustness and effectiveness of $\mathscr{L}_1$ adaptive control on the Vega platform (see Fig. 16).

8. Conclusions

From the results of this paper, we conclude that the TVC performance of the launch vehicle with $\mathscr{L}_1$ adaptive control offers several advantages: it improves transient response, provides better disturbance rejection, and reduces wind-induced oscillations, leading to faster adaptation and minimized structural vibrations. Moreover, the $\mathscr{L}_1$ adaptive controller demonstrates superior performance for the launchers, effectively managing time delays, structural flexibility, and unmodeled aerodynamic effects. Thus, the $\mathscr{L}_1$ controller enhances stability and robustness performances, making it an appropriate solution for future high-performance launch vehicle applications. Simulation results demonstrate that the $\mathscr{L}_1$ adaptive controller with the rigid launch vehicle accomplishes the stability requirements, robustness, and good transient and tracking performances. Also, the configuration with a Butterworth filter meets the stability requirements in the presence of flexible modes and provides good transient and tracking performance. Moreover, it was shown that the aerodynamic loads were within their specified safety limits in all cases analyzed.

The optimized $\mathscr{L}_1$-norm of $\left\|H(s)\left(1-C_f(s)\right)\right\|_{\mathcal{L}_1} L$ = 0.85 ensures a stability radius of approximately 18%. This optimization ensures that the angle of attack, pitch angle, and lateral velocity remain stable, thereby maintaining trajectory stability, which is critical for launch vehicle control. When we compare the performances between the responses in Figs. 9, 10, and 11, we conclude: The $\mathscr{L}_1$ provides uniform, guaranteed transient and steady-state bounds (under the $\mathscr{L}_1$-norm condition) and can maintain tracking and stability under fast, significant parameter changes that would require frequent re-scheduling in a fixed controller and in contrast with other design methods yields conservative but reliable margins for the assumed uncertainty range; it does not change online, so its performance under parameter excursions outside the modeled set can be poor. The plots in Figs. 14 and 15 illustrate the system's response over time, highlighting how the flexible and rigid-body launch vehicle dynamics react to the control input. In Fig. 15, the angle of attack α shows a rapid response, stabilizing around 0.08 rad. The pitch angle θ reacts slightly slower but stabilizes near the reference, while the lateral velocity gradually increases and stabilizes around 0.05 m/sec, reflecting the expected dynamics. Figure 16 demonstrates that in all analyzed cases, the aerodynamic loads remain within their specified safety limits.

Author Contributions

N.A.M. Naji developed the design methodology, numerical algorithms, wrote the original version of the manuscript, conducted the numerical simulations, analyzed and validated the results; A.-M. Stoica conceptualized the study, developed the algorithms for the design of the adaptive control system. Both authors discussed the results, reviewed, and approved the final version of the manuscript.

Acknowledgments

The authors express their appreciation to the anonymous reviewers for their constructive comments, remarks, and suggestions.

Conflict of Interest

The authors declared no potential conflict of interest concerning the research, authorship, and publication of the article.

Funding

The authors received no financial support for the research, authorship, and publication of this article.

Data Availability Statements

The datasets generated and/or analyzed during the current study are available from the corresponding author on reasonable request.

Nomenclature

L	The robustness radius [Dimensionless]	δ	The gimbal deflection angle [rad]
m	The vehicle mass [kg]	l_{GA}	The distance from the center of gravity to the aerodynamic center of pressure [m]
V	The launcher velocity [m/sec]	C_n	The coefficient of z-aerodynamic force [Dimensionless]
T	Thrust [N]	θ	The pitch angle [rad]
D	The drag force [N]	$\dot{z}$	Lateral drift speed [m/s]
G	The center of gravity [m]	α	The angle of attack [rad]
$r(t)$	Reference signal [rad]	α_w	The wind incidence [rad]
L_α	The aerodynamic force [N]		
ℓ_{CG}	Swivel Point C [m]		
I_{yy}	The pitch moment of inertia [kg · m^2]		

References

[1] Roux, C.R., Cruciani, I., *Control Law Robustness: in Atmospheric Flight of the Vega Launcher*, ESA GNC, 2009.
[2] Navarro-Tapia, D., Marcos, A., Bennani, S., Roux, C., Joint robust structured design of VEGA launcher's rigid-body controller and bending filter, *69th International Astronautical Congress 2018, International Astronautical Federation (IAF)*, Bremen, Germany, 1-5, 2018.
[3] Orr, J.S., Wall, J.H., VanZwieten, T.S., Hall, C.E., Space launch system ascent flight control design, *In 2014 American Astronautical Society (AAS) Guidance, Navigation, and Control Conference (No. M14-3168)*, 2014.
[4] Jang, A.J., Alaniz, W., Hall, R., Bedrossian, N., Hall, C., Jackson, M., Design of launch vehicle flight control systems using ascent vehicle stability analysis tool, *In AIAA Guidance, Navigation, and Control Conference*, p. 6652, 2011.

[5] Griffin, B.J., Burken, J.J., Xargay, E., $\mathscr{L}1$ adaptive control augmentation system with application to the X-29 lateral/directional dynamics: A multi-input multi-output approach, *In AIAA Guidance, Navigation, and Control Conference*, p. 7687, 2010.

[6] Naji, N.A.M., Stoica, A.-M., Design of a robust controller for the VEGA TVC using the L1-Adaptive Control, *INCAS Bulletin*, 15(4), 2023, 175–185.

[7] Atmaja, B.K., Joelianto, E., Surface control design of rocket using MIMO PID robust integral backstepping, *ICA, Bandung*, Indonesia,162–169, 2011.

[8] Marcos, A., Bennani, S., Roux, C., Valli, M., LPV modelling and LFT Uncertainty Identification for Robust Analysis: application to the VEGA Launcher during Atmospheric Phase, *In IFAC- University of Bristol – Bristol Research Portal LP*, 48(26), 2015, 115–120.

[9] Simplício, P., Bennani, S., Marcos, A., Roux, C., Lefort, X., Structured singular-value analysis of the Vega launcher in atmospheric flight, *Journal of Guidance, Control, and Dynamics*, 39(6), 2016, 1342–1355.

[10] Mihaly, V., Su, M., µ -Synthesis for Fractional-Order Robust Controllers, *Mathematics*, 9(8), 2021, 1-21.

[11] Wall, J.H., Orr, J.S., VanZwieten, T.S., Space launch system implementation of adaptive augmenting control, *Advances in Astronautical Sciences*, 151, 2014, 225–239.

[12] Navarro-Tapia, S.B.D., Marcos, A., Envelope extension via adaptive augmented thrust vector control system, *Journal of Guidance, Control, and Dynamics*, 44(5), 2021, 1044–1052.

[13] Cao, C., Hovakimyan, N., Design and analysis of a novel $\mathscr{L}1$ adaptive control architecture with guaranteed transient performance, *IEEE Transactions on Automatic Control*, 53(2), 2008, 586–591.

[14] Cao, C., Hovakimyan, N., Stability margins of $\mathscr{L}1$ adaptive controller: Part II, *Proc. Am. Control Conf.*, United States, New York, 3931–3936, 2007.

[15] Hovakimyan, N., Cao, C., L1 Adaptive Control Theory Guaranteed Robustness with Fast Adaptation, *Connecticut Society for Industrial and Applied Mathematics Philadelphia*, Philadelphia, 2010.

[16] Palhares, R.M., Peres, P.L.D., Ramírez, J.A., A Linear Matrix Inequality Approach to The Peak-to-Peak Guaranteed Cost Filtering Design, *IFAC Proceedings*, 33(14), 2000, 29–34.

[17] Nazin, S.A., Polyak, B.T., Topunov, M.V., Rejection of bounded exogenous disturbances by the method of invariant ellipsoids, *Automation and Remote Control*, 68(3), 2007, 467–486.

[18] Venkatesh, S.R., Dahleh, M.A., Does star norm capture l1 norm?, *in American Control Conference*, Seattle, WA, 944–945, 1995.

[19] Löfberg, J., YALMIP: A toolbox for modeling and optimization in MATLAB, *Proceedings of the IEEE International Symposium on Computer-Aided Control System Design*, 2004.

[20] Rowell, L.F., Korte, J.J., Launch Vehicle Design and Optimization Methods and Priority for the Advanced Engineering Environment, No. NASA/TM-2003-212654, Hampton, Virginia, 2003.

[21] Gadea Díaz, E., *Design of a robust controller for the VEGA TVC using the u-synthesis\technique*, Master's Thesis, UPC-ETSEIB, Dublin, 2012.

[22] Navarro-Tapia, D., Marcos, A., Bennani, S., Roux, C., Performance and robustness trade-off capabilities for the VEGA launcher TVC system, *European Conference for Aeronautics and Space Sciences*, Bristol, BS8 1TR, United Kingdom, 2019.

[23] Zarchan, P., Tactical and Strategic Missile Guidance, *American Institute of Aeronautics and Astronautics*, 2007.

[24] Boglis, C., Stoica, A.M., Adaptive control methods for launch vehicles, Ph.D. Thesis, Universitatea Politehnica din Bucure s ti Metode de Control Adaptiv Pentru Vehicule Lansatoare, Romania, 2023.

[25] Bennani A. et al., Robust TVC for Flexible Rockets, *ESA Conference on Flight Control*, 2019.

[26] Simplício, P., Bennani, S., Marcos, A., Roux, C., Lefort, X., Structured Singular Value Analysis of the VEGA Launcher in Atmospheric Flight, *Journal of Guidance, Control, and Dynamics*, 39(6), 2016, 1342-1355.

[27] Clement, B., Duc, G., Mauffrey, S., Aerospace launch vehicle control: A gain scheduling approach, *Control Engineering Practice*,13(3), 2005, 333–347.

[28] Naji, N.A.M., Stoica, A.-M., $\mathscr{L}1$ adaptive control design for the rigid body launch vehicle, *INCAS Bulletin*, 15(4), 2023, 187–197.

[29] Naji, N.A.M., Stoica, A.-M., $\mathscr{L}1$ adaptive controller of VEGA Launcher subject to flexible modes, *INCAS Bulletin*, 16(4), 2024, 81–89.

ORCID iD

Naji Anees Muqdad NAJI https://orcid.org/0000-0002-0083-7930

Adrian-Mihail STOICA https://orcid.org/0000-0001-5369-8615

How to cite this article: NAJI N.A.M., STOICA A.-M. On the $\mathscr{L}1$ Norm Minimization in Adaptive Control of Launch Vehicles, *J. Appl. Comput. Mech.*, xx(x), 2026, 1–14. https://doi.org/10.22055/jacm.2025.48377.5191